Supplemental Files

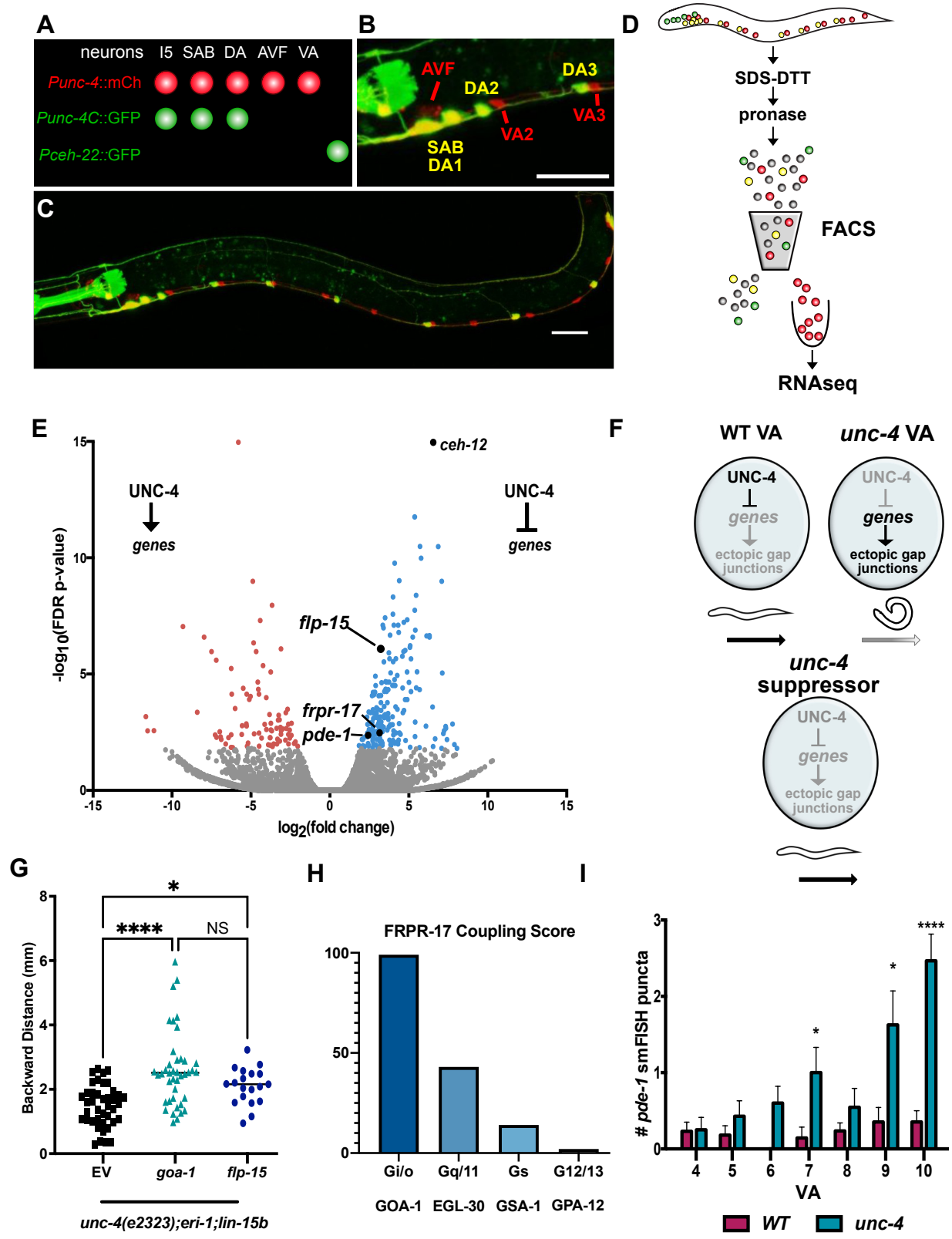

Supplemental Figure 1: Cell-specific RNA sequencing strategy to identify UNC-4 target genes that regulate wiring, related to Figure 1.

A. Intersectional labeling strategy to enrich for VA motor neurons. The *unc-4* promoter (*Punc-4::*mCh) driving mCherry labels (red) I5, SAB, DA, AVF and VA neurons. A truncated *unc-4* promoter (*Punc-4C*::GFP) driving GFP labels (green) I5, SAB and DA neurons. As a result, VA and AVF are exclusively labeled with mCherry (red) and VA neurons (12) outnumber AVF neurons (2) by ratio of 6:1. Confocal images of anterior region (**B**) and full length (**C**) L2 stage larva illustrating intersectional labeling strategy. Pharyngeal muscle (green) is labeled with co-selectable marker (*myo-2::*GFP). Scale bars = 20µm.

D. Strategy for isolating VA motor neurons for RNA-seq. Synchronized L2-stage larvae were dissociated to single cells for FACS-isolation of red-only (VA-enriched) cells and RNA-Seq.

E. Volcano plot of upregulated (> 2X, FDR p-value < .01) (blue dots) and downregulated (< -2X, FDR p-value <.01) (red dots) transcripts in *unc-4* mutant VAs versus wild-type VAs (see Methods). Black dots denote suppressors of the Unc-4 movement defect.

F. Genetic strategy to identify Unc-4 "suppressor" genes. In wild-type (WT) VAs (**top left**), UNC-4 blocks expression of genes that can induce ectopic gap junctions and disrupt backward movement. In *unc-4* mutant VAs (**top right**), UNC-4 target genes are de-repressed resulting in ectopic gap junction formation and disrupted backward movement. RNAi or genetic knockdown of an UNC-4 target gene can prevent the formation ectopic gap junctions and restore backward movement thus resulting in "suppression" of the Unc-4 mutant phenotype.

G. RNAi knock down of either *flp-15* or *goa-1* partially restores backward locomotion to an *unc-4* mutant. Backward distance traveled in a 3-minute period by *unc-4(e2323);eri-1;lin-15b* in empty vector (EV) control (black) (n = 41), *goa-1* (teal) (n=41) or *flp-15* (blue) (n=20) feeding RNAi treatments. One-way ANOVA, * p = 0.0368, **** = p < 0.0001. Data are mean +/- SE.

H. PREDCouple2 prediction of FRPR-17 G-protein coupling. FRPR-17 is predicted (Score 99) to couple with Gi/o with lower scores for other classes of G-proteins. Names of corresponding G-proteins in *C. elegans* are listed below.

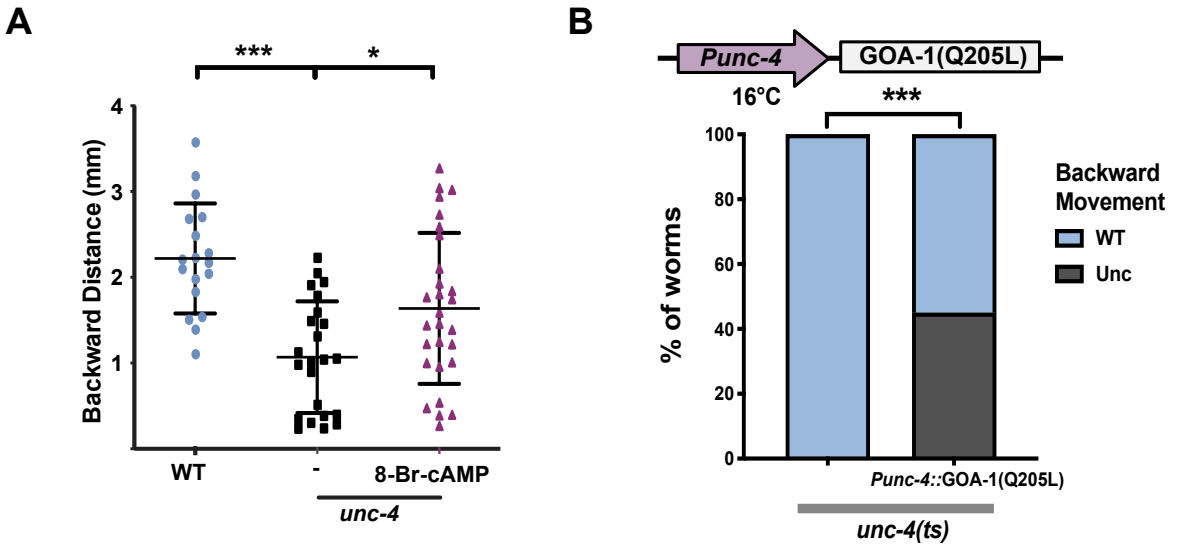

Supplemental Figure 2: cAMP signaling in VA neurons promotes backward movement, related to Figure 3.

A. Backward distance traveled in a 3-minute period of wild type (light blue), *unc-4* (black) and *unc-4* + 8-Br-cAMP (maroon). Growth on 8-Br-cAMP partially restores backward locomotion to *unc-4(e2323)* mutant animals. One-way ANOVA, N > 15 for each genotype. * p = 0.0169, **** = p < 0.0001.

B. GOA-1/GαO activation in VA neurons enhances the Unc-4 backward movement defect. The *Punc-4* promoter was used to drive expression of constitutively active GOA-1(Q205L) in VAs in *unc-4(ts)* worms. At 16°C, *unc-4(ts)* worms show wild type (WT) backward locomotion whereas *unc-4(ts)* worms that express GOA-1(Q205L) in VAs show uncoordinated (Unc) backward movement in the tapping assay. Fisher's Exact test. *** = p< 0.001. N>50 for each genotype. *unc-4(ts)* = *unc-4(e2322)* and is temperature sensitive.

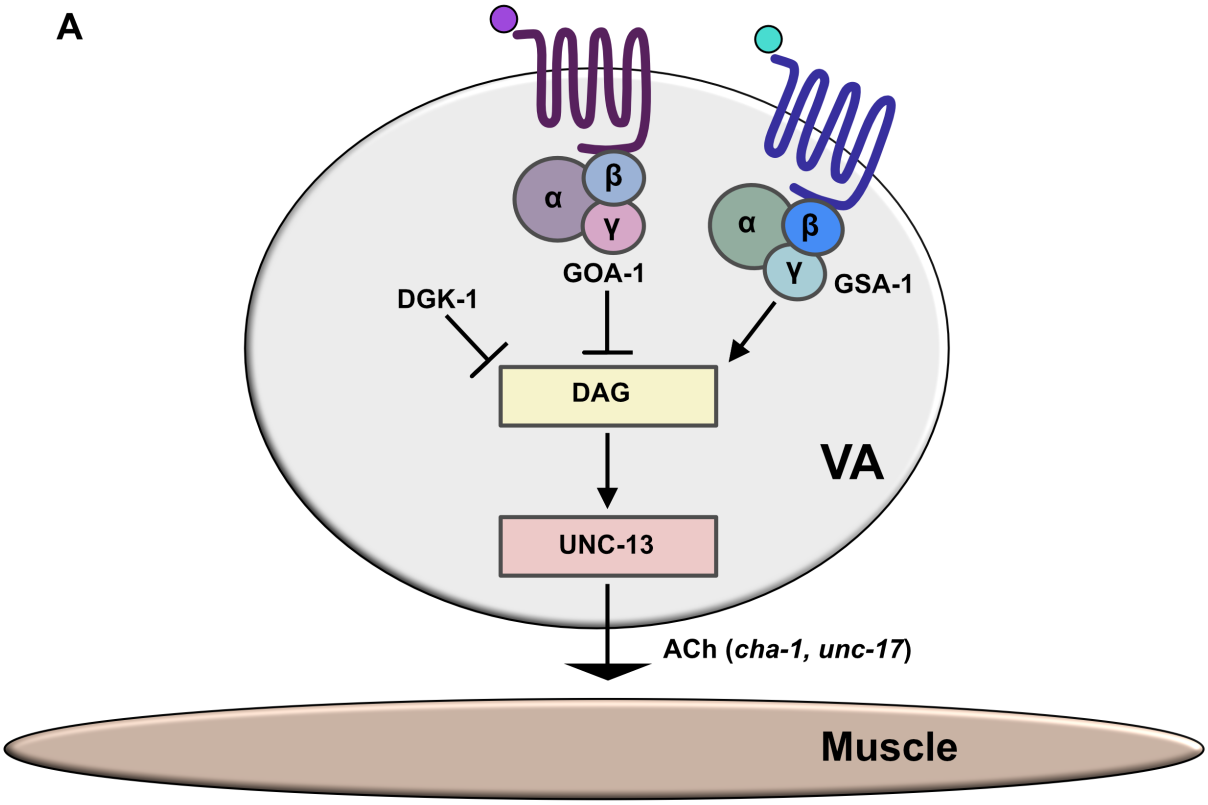
A
α
β
γ
GOA-1
α
β
γ
GSA-1
DGK-1
DAG
VA
UNC-13
ACh (cha-1, unc-17)
Muscle

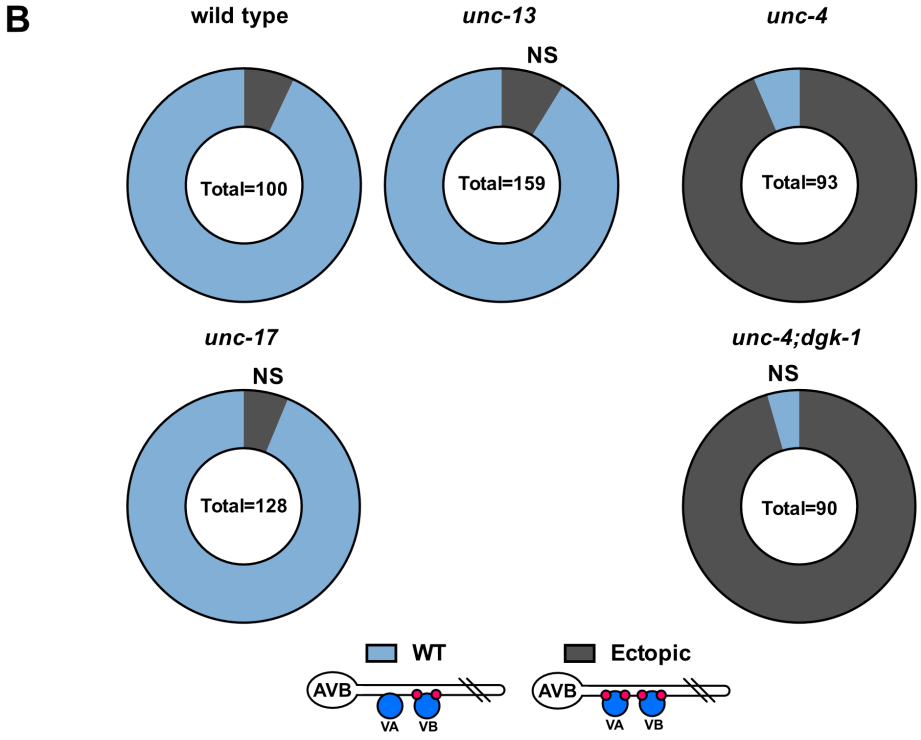
B
wild type
unc-13
NS
unc-4
Total=100
Total=159
Total=93
unc-17
NS
unc-4;dgk-1
NS
Total=128
Total=90
WT
Ectopic
AVB
VA
VB
AVB
VA
VB

Supplemental Figure 3: Cholinergic release at the neuromuscular Junction does not affect gap junction specificity of VAs, related to Figure 3.

A. Acetylcholine (Ach) release at the neuromuscular junction is regulated by GOA-1 and GSA-1. GOA-1 antagonizes DGK- 1/diacylglycerol kinase to inhibit DAG production. GSA-1 functions through ACY-1/adenylyl cyclase and cAMP (not shown) to promote DAG binding to UNC-13, which is required for synaptic vesicle fusion. Thus, GOA-1 activity inhibits Ach release whereas GSA-1 promotes Ach release. Genetic ablation of *unc-13* or *unc-17* should result in reduced Ach signaling whereas loss of *dgk-1* should upregulate Ach release.

B. (**Left**) Percentage of VAs miswired with AVB gap junctions in wild type, *unc-13(e51)* mutants and *unc-17(e113)* mutants. Genetic ablation of neither *unc-13* nor *unc-17* results in ectopic VA→AVB gap junctions. (**Right**) Percentage of VAs with ectopic VA→AVB gap junctions in *unc-4(e120)* mutants, and *unc-4;dgk-1* double mutants. Loss of *dgk-1* does not suppress the *unc-4* miswiring defect. Fisher's Exact test, NS = Not Significant.

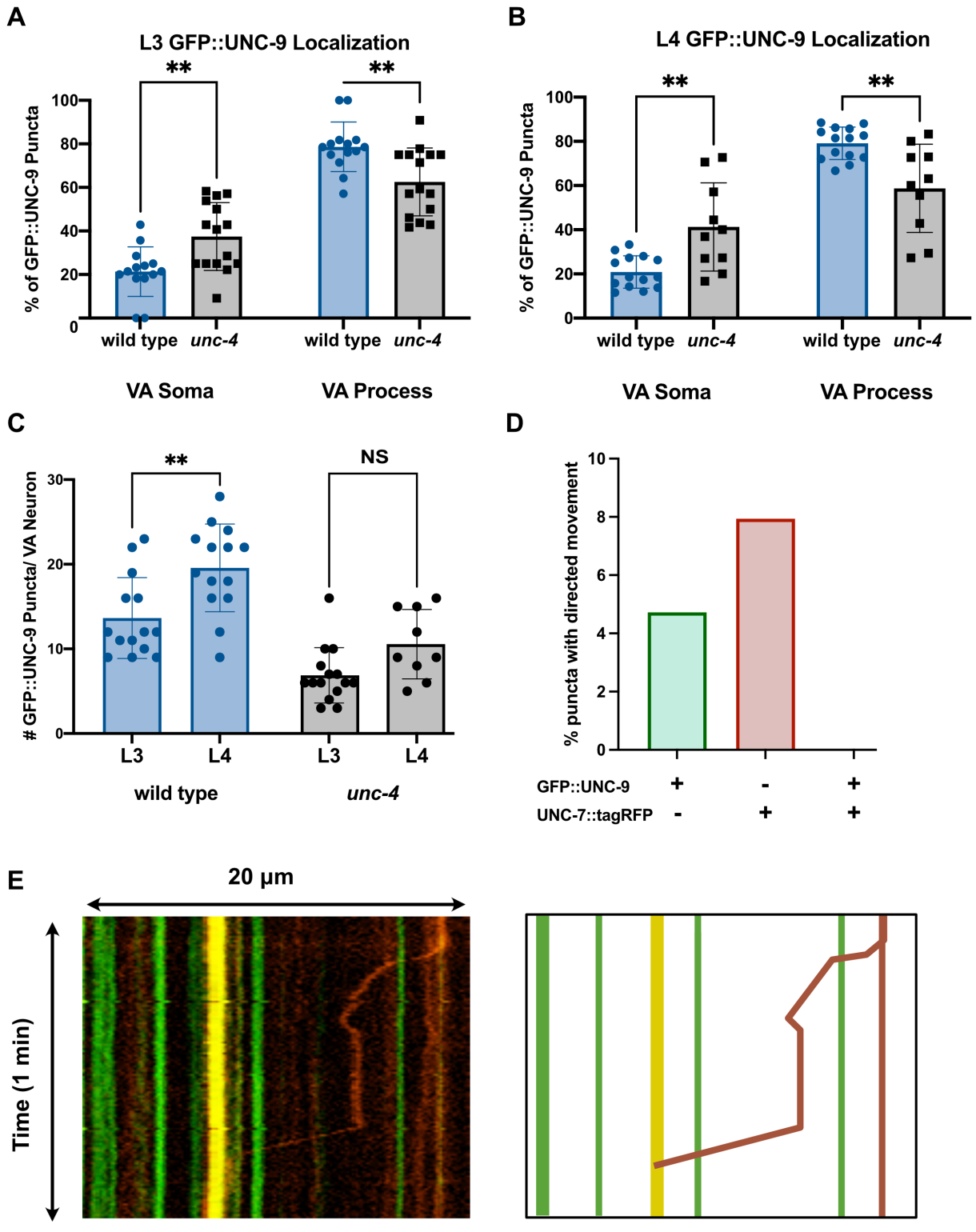
A
L3 GFP::UNC-9 Localization
% of GFP::UNC-9 Puncta
**
**
wild type
unc-4
wild type
unc-4
VA Soma
VA Process
B
L4 GFP::UNC-9 Localization
% of GFP::UNC-9 Puncta
**
**
wild type
unc-4
wild type
unc-4
VA Soma
VA Process
C
GFP::UNC-9 Puncta/ VA Neuron
**
NS
L3
L4
L3
L4
wild type
unc-4
D
% puncta with directed movement
GFP::UNC-9 + - +
UNC-7::tagRFP - + +
E
20 µm
Time (1 min)

Supplemental Figure 4. Dual-color labeling strategy tracks presumed VA→AVA gap junctions, related to Figure 4.

A. Subcellular localization of GFP::UNC-9 in VA motor neurons at the L3 larval stage in wild type (blue) and *unc-4* mutants (black). *unc-4* mutant VAs show significantly more GFP::UNC-9 puncta in the VA cell soma and significantly fewer GFP::UNC-9 puncta in the VA axon compared to wild type, as predicted by EM reconstruction (White et al., 1986, 1992). Two-way ANOVA used to determine significance. ** = $p < 0.001$. N = 15 for each group.

B. Subcellular localization of GFP::UNC-9 in VA motor neurons at the L4 stage in wild type (blue) and *unc-4* mutants (black). *unc-4* mutant VAs shown significantly more GFP::UNC-9 puncta in VA cell soma and significantly fewer GFP::UNC-9 puncta in the VA axon compared to wild type. Two-way ANOVA used to determine significance. ** = $p < 0.001$. N >10 for each group.

C. GFP::UNC-9 puncta in the VA axon in wild type (blue) and *unc-4* mutant (black). In the wild type, significantly more GFP::UNC-9 puncta are detected in the VA axon in L4 vs L3 stage larva whereas the number of GFP::UNC-9 puncta in the VA axon of *unc-4* mutants is not elevated during development from the L3 to L4 larval stage. Two-way ANOVA used to determine significance. ** = $p < 0.001$. NS = Not Significant. N >10 for each group. *unc-4(e2323)* used in all experiments.

D. Percent of puncta with directed locomotion for *punc-4::*GFP::UNC-9 (green), UNC-7::tagRFP (red), or dual-labeled puncta. Puncta labeled with both *punc-4::*GFP::UNC-9 and UNC-7::tagRFP were entirely stationary over 30 minutes. N = 10 VA neurons.

E. (left) Representative kymograph of dual-color live cell images of *punc-4::GFP::UNC-9* (green) in VA motor neurons and UNC-7::tagRFP (red) in AVA. Example of mobile UNC-7::tagRFP puncta. Dual-labeled (GFP::UNC-9 + UNC-7::tagRFP) punctum (yellow) is stationary. (**right)** Tracing of kymograph.

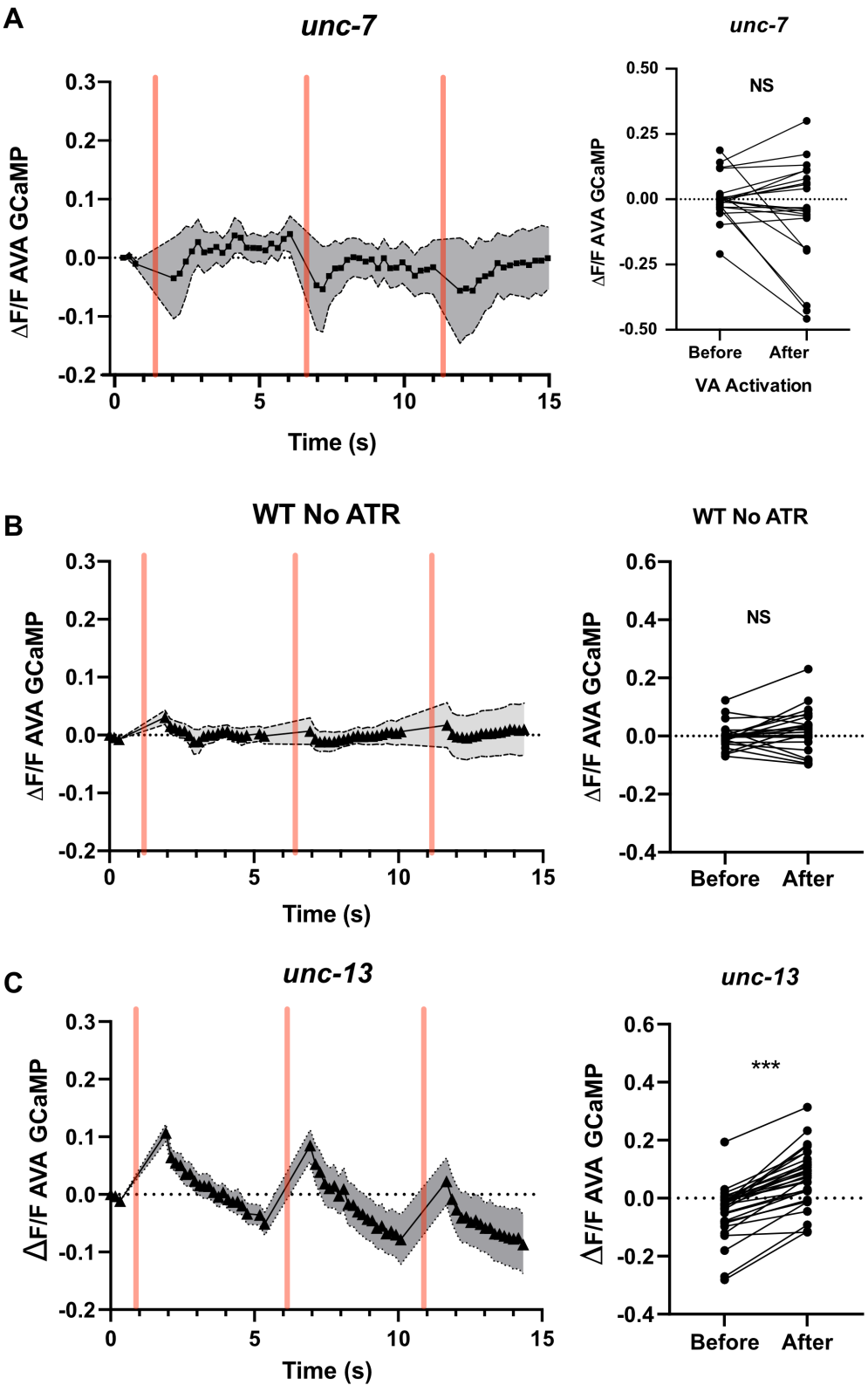
A
unc-7
ΔF/F AVA GCaMP
Time (s)
unc-7
NS
ΔF/F AVA GCaMP
Before
After
VA Activation
B
WT No ATR
ΔF/F AVA GCaMP
Time (s)
WT No ATR
NS
ΔF/F AVA GCaMP
Before
After
C
unc-13
ΔF/F AVA GCaMP
Time (s)
unc-13
***
ΔF/F AVA GCaMP
Before
After

Supplemental Figure 5: Detection of functional VA→AVA electrical synapses, related to Figure 5.

A. Functional VA→AVA electrical synapses are not detected when VA→AVA gap junction assembly is disrupted in *unc-7* mutants (Starich et al., 2009). (**left**) Quantification of AVA::GCaMP6s fluorescence in *unc-7(e5)*. Three successive VA activations (500 ms) are denoted by pink vertical bars. Shaded area = SEM. N = 9 worms. (**Right**) Quantification of $\Delta F/F_0$ before versus after 561 stimulation. Paired t-test. N = 9 worms, 18 activations. NS = Not Significant.

B. AVA::GCaMP response depends on VA activation. Calcium influx in AVA is not detected in wild-type worms grown in the absence of ATR, the necessary cofactor for Chrimson. (**left**) Quantification of wild type (-ATR) AVA::GCaMP6s fluorescence. Three successive VA activations (500 ms) are denoted by pink vertical bars. Shaded area = SEM. N = 9 worms. (**Right**) Quantification of $\Delta F/F_0$ before versus after 561 stimulation. Paired t-test. N = 9 worms, 18 activations. NS = Not Significant.

C. Functional VA→AVA electrical synapses are detected in *unc-13* mutants in which chemical synaptic release is disabled. (**left**) Quantification of AVA::GCaMP6s fluorescence in *unc-13(e51)*. Three successive VA activations (500 ms) are denoted by pink vertical bars. Shaded area = SEM. N = 9 worms. (**Right**) Quantification of $\Delta F/F_0$ before versus after 561 stimulation. Paired t-test. N = 9 worms, 18 activations. *** $p < 0.001$.

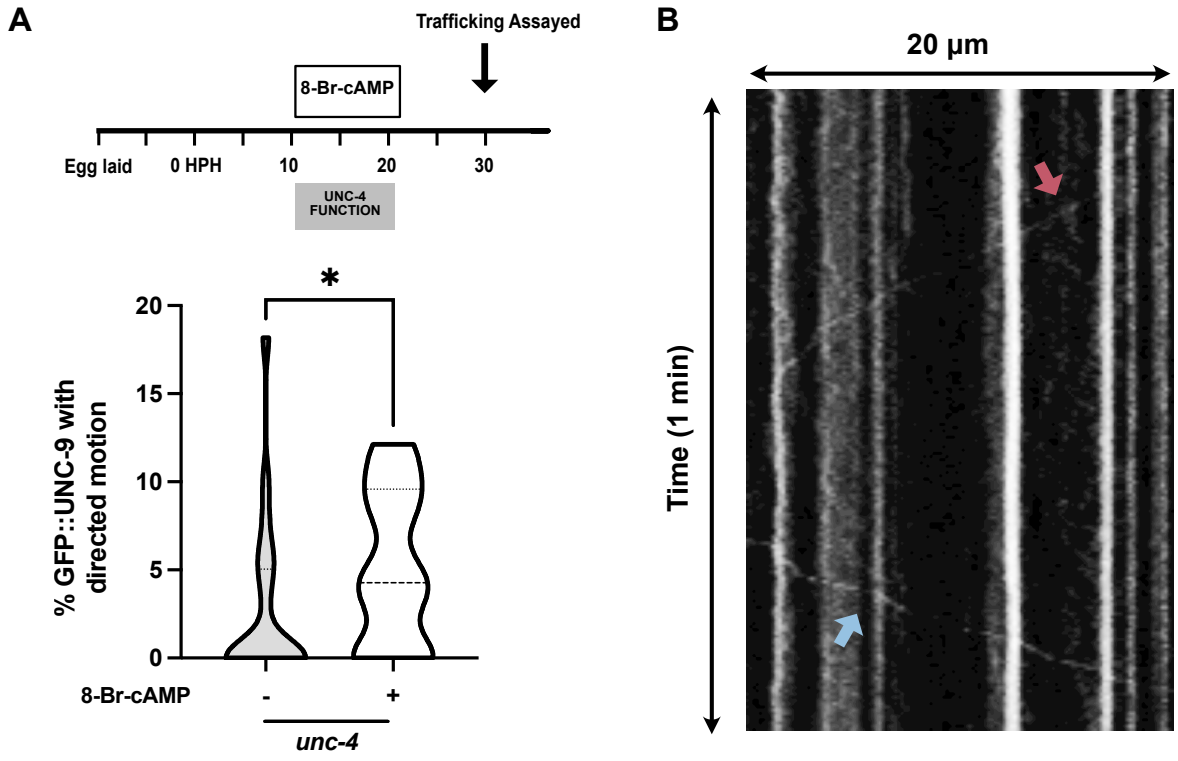

Supplemental Figure 6: Elevated cAMP restores trafficking of GFP::UNC-9, related to Figure 6.

A. (**top**) *unc-4* mutant larvae were treated with 8-Br-cAMP during the larval developmental period in which *unc-4* function is required for VA motor circuit wiring. *unc-4(e2323)* larvae expressing *Punc-4::GFP::UNC-9* were fed 8-Br-cAMP for 10 hours during the L2-L3 larval period. (**bottom**) Quantification of GFP::UNC-9 movement in *unc-4* worms that were either treated (+) or not treated (-) with 8-Br-cAMP. (-) data are the same as in Figure 6B. Data are percent of motile puncta in a 3-minute period for given VA. N > 15 for each group. Mann-Whitney test. * p= 0.0481
Results from VA2, VA3, VA4. **B)** Representative kymograph of GFP::UNC-9 in *unc-4* worms fed 8-Br-cAMP depict anterograde (red arrow) and retrograde tracks of GFP::UNC-9.

Supplemental Table 1: Genes tested for suppression of backward locomotion defect of *unc-4(e2323)*, related to Figure 1.

Gene Tested for Backward Suppression	Method	Suppressed?
acr-15	RNAi	
asah-1	RNAi	
C30B5.7	RNAi	
C30F12.5	RNAi	
C34C6.7	RNAi	
C35E7.2	RNAi	
C35E7.4	RNAi	
C47D2.1	RNAi	
ccb-2	RNAi	
ceh-12	Mutant and RNAi	Yes
ceh-24	RNAi	
ceh-31	RNAi	
ces-1	RNAi	
ckr-1	Mutant	
cof-2	RNAi	
cup-4	RNAi	
D2024.4	RNAi	
exc-5	RNAi	
F10B5.3	RNAi	
F11E6.6	RNAi	
F14F11.2	RNAi	
F26B1.1	RNAi	
F32f2.1	RNAi	
F34D10.4	RNAi	
F42A8.1	RNAi	
F43G6.4	RNAi	
F44G4.7	RNAi	
flp-1	Mutant	
flp-10	RNAi	
flp-15	RNAi	Yes
flp-9	RNAi	
frpr-15	RNAi	
frpr-17	Mutant and RNAi	Yes

gcy-11	RNAi	
gcy-15	RNAi	
gcy-21	RNAi	
glr-2	RNAi	
hil-7	RNAi	
K01A2.3	RNAi	
K01A6.6	RNAi	
K07D4.5	RNAi	
lec-2	RNAi	
lim-4	RNAi	
lim-7	RNAi	
lin-12	RNAi	
lin-31	RNAi	
nlp-12	RNAi	
nlp-15	RNAi	
nlp-38	RNAi	
nlp-40	RNAi	
pax-2	RNAi	
pct-1	RNAi	
pde-1	Mutant	Yes
prkl-1	Mutant	
R05G6.10	RNAi	
R06C1.6	RNAi	
rgs-3	RNAi	
sem-4	RNAi	
ser-5	Mutant	
sod-4	RNAi	
sue-1	RNAi	
T19C3.5	RNAi	
T23G7.3	RNAi	
unc-122	RNAi	
unc-129	RNAi	
unc-30	RNAi	
unc-71	RNAi	
unc-86	RNAi	
vab-23	RNAi	
vab-8	Mutant	
W04A8.4	RNAi	
Y43C5A.3	RNAi	

Y47H9A.1	RNAi	
ZC581.3	RNAi	
zig-5	RNAi	
zip-8	RNAi	
ZK265.7	RNAi	

Supplemental Table 2: Adjacent neurons that fail to form electrical synapses, related to Figure 1. Tab 1: List of pairs of neurons that form chemical synapses but not electrical synapses. This list does not include neurons that are in physical contact but do not form electrical synapses and therefore likely underestimates the number of neurons that are in physical contact and express compatible innexins but do not form gap junctions. Tab 2: Neurons from Tab 1 color-coded for expression of the innexins UNC-7 and UNC-9 (Bhattacharya et al., 2019). Over 600 neurons express compatible innexins and physically contact one another (based on presence of chemical synapses) but do not form gap junctions.

Supplemental Table 3: *C. elegans* strains used in study, related to STAR Methods.

REAGENT or RESOURCE	SOURCE	IDENTIFIER
wdis54	Von Stetina, 2007, Figure 1B, 2H, 3F	NC1809
unc-4(e2323); wdis54	Von Stetina, 2007, Figure 1B, 2H, 3E	NC1939
unc-4(e2323)	Winnier et al., 1999, Figure 1C, 2B, 3C	NC2289
unc-4::mCh unc-4c::gfp	Figure 1D, Figure S1	NC2957
unc-4(e120); unc-4::mCh unc-4c::GFP	Figure 1D, Figure S1	NC2958
unc-4(e2323);eri-1;lin-15b	Von Stetina, 2007, Figure 1D, Figure S2	NC1558
unc-4(e2322)	Miller et al., 1992, Figure 2B	
unc-4(e2322);pde-1	Figure 2B	NC3771
unc-4(e2322);frpr-17	Figure 2B	NC3763
unc-4(e2323);pde-1;wdis54	Figure 2H	NC3772
unc-4(e2323);frpr-17;wdis55	Figure 2H	NC3764
bnc-1::GFP	Oliver Hobert Lab, Figure 2D, 2F	OH15624
unc-4(e120);bnc-1::GFP	Figure 2D, 2F	NC3664
unc-4(e2323);goa-1;wdis54	Figure 3D, E	NC3765
unc-4(e2323);gsa-1(gof);wdis54	Figure 3D, E	NC2456
unc-4(e2323;acy-1(gof);wdis54	Figure 3D, E	NC3774
unc-4(e2323);goa-1	Figure 3C	NC3773
unc-13;wdis54	Figure S3	NC2300
unc-17;wdis54	Figure S3	NC2444

unc-4(e120);dgk-1;wdis54	Figure S3	NC2755
unc-4(e120);wdis54	Figure 3I, Figure S3	NC1813
unc-4(e2323);Punc-17::bPAC	Figure 3G	NC3815
EX[Punc-4::PDE-4]	Figure 3H	NC3670
unc-4(e2322);EX[Punc-4::GOA-1(gof)]	Figure S2	NC2367
unc-4(e120);goa-1; wdis54	Figure 3I	NC2010
unc-4(e120);goa1;EX[Punc-4::GOA-1]; wdis54	Figure 3I	NC2608
unc7::frt_stop_frt_tagRFP;EX[Pflp-18::flppase, Punc-4::GFP::UNC-9]	Figure 4B-E, 7B	NC3775
unc-4(e2323);unc-7::frt_stop_frt_tagRFP;EX[Pflp-18::flppase, Punc-4::GFP::UNC-9]	Figure 4B-C, 7B	NC3789
unc-4(e2323);goa-1;unc-7::frt_stop_frt_tagRFP;EX[Pflp-18::flppase, Punc-4::GFP::UNC-9]	Figure 4B-C	NC3790
unc4::Chrim;EX[Pflp18::GCaMP6s]	Figure 5C	NC3666
unc-4(e2323);unc-4::Chrim;EX[Pflp18::GCaMP6s]	Figure 5D	NC3667
unc-4(e2323);goa-1;unc-4::Chrim;EX[Pflp18::GCaMP6s]	Figure 5E	NC3669
unc-7;unc-4::Chrim;EX[Pflp18::GCaMP6s]	Figure S6	NC3668
EX[Punc-4::GFP::UNC-9]	Figure 6, 7, Figure S4	NC3653
unc-4(e2323);EX[Punc-4::GFP::UNC-9]	Figure 6, 7, Figure S4, S5	NC3654
unc-4(e2323);goa-1;EX[Punc-4::GFP::UNC-9]	Figure 6	NC3816